J|A|C|S
ARTICLES
Published on Web 10/09/2007

Probing the Electronic Structure of Early Transition-Metal Oxide Clusters: Polyhedral Cages of $(V_2O_5)_n^-$ ($n = 2-4$) and $(M_2O_5)_2^-$ (M = Nb, Ta)

Hua-Jin Zhai,[†,‡] Jens Döbler,[§] Joachim Sauer,*[,§] and Lai-Sheng Wang*[,†,‡]

Contribution from the Department of Physics, Washington State University, 2710 University Drive, Richland, Washington 99354, Chemical & Materials Sciences Division, Pacific Northwest National Laboratory, MS K8-88, P.O. Box 999, Richland, Washington 99352, and Institut für Chemie, Humboldt Universität Berlin, Unter den Linden 6, 10099 Berlin, Germany

Received July 9, 2007; E-mail: js@chemie.hu-berlin.de; ls.wang@pnl.gov

Abstract: Vanadium oxide clusters, $(V_2O_5)_n$, have been predicted to possess interesting polyhedral cage structures, which may serve as ideal molecular models for oxide surfaces and catalysts. Here we examine the electronic properties of these oxide clusters via anion photoelectron spectroscopy for $(V_2O_5)_n^-$ ($n = 2-4$), as well as for the 4d/5d species, $Nb_4O_{10}^-$ and $Ta_4O_{10}^-$. Well-resolved photoelectron spectra have been obtained at 193 and 157 nm and used to compare with density functional calculations. Very high electron affinities and large HOMO−LUMO gaps are observed for all the $(V_2O_5)_n$ clusters. The HOMO−LUMO gaps of $(V_2O_5)_n$, all exceeding that of the band gap of the bulk oxide, are found to increase with cluster size from $n = 2-4$. For the M_4O_{10} clusters, we find that the Nb/Ta species yield similar spectra, both possessing lower electron affinities and larger HOMO−LUMO gaps relative to V_4O_{10}. The structures of the anionic and neutral clusters are optimized; the calculated electron binding energies and excitation spectra for the global minimum cage structures are in good agreement with the experiment. Evidence is also observed for the predicted trend of electron delocalization versus localization in the $(V_2O_5)_n^-$ clusters. Further insights are provided pertaining to the potential chemical reactivities of the oxide clusters and properties of the bulk oxides.

1. Introduction

Transition-metal oxides are of extensive current interests in chemical, materials, and surface sciences because of their diverse physicochemical properties and technological applications.[1] In particular, group VB metal oxides are widely used as catalysts for important industrial chemical transformations,[2−5] such as $SO_2 \rightarrow SO_3$ oxidation and selective reduction of nitric oxide by ammonia or hydrocarbon conversions. To help elucidate the microscopic details of the catalytic processes, experimental and theoretical works have been performed on vanadium oxide clusters in the past decade.[6−15] Indeed, gas-phase studies in combination with high-level calculations have emerged as a powerful approach toward mechanistic insights into the complex metal oxide surfaces and catalytic processes at the molecular level.[16,17]

[†] Washington State University.
[‡] Pacific Northwest National Laboratory.
[§] Humboldt Universität Berlin.

(1) Rao, C. N. R.; Raveau, B. *Transition Metal Oxides*; Wiley-VCH: New York, 1995.
(2) (a) Wachs, I. E.; Chen, Y.; Jehng, J. M.; Briand, L. E.; Tanaka, T. *Catal. Today* **2003**, *78*, 13. (b) Wachs, I. E.; Briand, L. E.; Jehng, J. M.; Burcham, L.; Gao, X. *Catal. Today* **2000**, *57*, 323.
(3) (a) Weckhuysen, B. M.; Keller, D. E. *Catal. Today* **2003**, *78*, 25. (b) Surnev, S.; Ramsey, M. G.; Netzer, F. P. *Prog. Surf. Sci.* **2003**, *73*, 117.
(4) Ziolek, M. *Catal. Today* **2003**, *78*, 47.
(5) Ushikubo, T. *Catal. Today* **2000**, *57*, 331.
(6) (a) Vyboishchikov, S. F.; Sauer, J. *J. Phys. Chem. A* **2001**, *105*, 8588. (b) Vyboishchikov, S. F.; Sauer, J. *J. Phys. Chem. A* **2000**, *104*, 10913.
(7) Calatayud, M.; Andres, J.; Beltran, A. *J. Phys. Chem. A* **2001**, *105*, 9760.
(8) (a) Bell, R. C.; Zemski, K. A.; Kerns, K. P.; Deng, H. T.; Castleman, A. W., Jr. *J. Phys. Chem. A* **1998**, *102*, 1733. (b) Zemski, K. A.; Justes, D. R.; Bell, R. C.; Castleman, A. W., Jr. *J. Phys. Chem. A* **2001**, *105*, 4410. (c) Justes, D. R.; Mitric, R.; Moore, N. A.; Bonacic-Koutecky, V.; Castleman, A. W., Jr. *J. Am. Chem. Soc.* **2003**, *125*, 6289.
(9) (a) Wu, H.; Wang, L. S. *J. Chem. Phys.* **1998**, *108*, 5310. (b) Zhai, H. J.; Wang, L. S. *J. Chem. Phys.* **2002**, *117*, 7882.
(10) (a) Dinca, A.; Davis, T. P.; Fisher, K. J.; Smith, D. R.; Willett, G. D. *Int. J. Mass Spectrom.* **1999**, *182*, 73. (b) Jackson, P.; Fisher, K. J.; Willett, G. D. *Chem. Phys.* **2000**, *262*, 179.
(11) (a) Asmis, K. R.; Brümmer, M.; Kaposta, C.; Santambrogio, G.; von Helden, G.; Meijer, G.; Rademann, K.; Wöste, L. *Phys. Chem. Chem. Phys.* **2002**, *4*, 1101. (b) Asmis, K. R.; Meijer, G.; Brümmer, M.; Kaposta, C.; Santambrogio, G.; Wöste, L.; Sauer, J. *J. Chem. Phys.* **2004**, *120*, 6461.
(12) Molek, K. S.; Jaeger, T. D.; Duncan, M. A. *J. Chem. Phys.* **2005**, *123*, 144313.
(13) Asmis, K. R.; Santambrogio, G.; Brümmer, M.; Sauer, J. *Angew. Chem., Int. Ed.* **2005**, *44*, 3122.
(14) Janssens, E.; Santambrogio, G.; Brümmer, M.; Wöste, L.; Lievens, P.; Sauer, J.; Meijer, G.; Asmis, K. R. *Phys. Rev. Lett.* **2006**, *96*, 233401.
(15) (a) Dong, F.; Heinbuch, S.; He, S. G.; Xie, Y.; Rocca, J. J.; Bernstein, E. R. *J. Chem. Phys.* **2006**, *125*, 164318. (b) Matsuda, Y.; Bernstein, E. R. *J. Phys. Chem. A* **2005**, *109*, 3803.
(16) For selected examples, see: (a) Waters, T.; O'Hair, R. A.; Wedd, A. G. *J. Am. Chem. Soc.* **2003**, *125*, 3384. (b) Zhai, H. J.; Kiran, B.; Cui, L. F.; Li, X.; Dixon, D. A.; Wang, L. S. *J. Am. Chem. Soc.* **2004**, *126*, 16134. (c) Huang, X.; Zhai, H. J.; Waters, T.; Li, J.; Wang, L. S. *Angew. Chem., Int. Ed.* **2006**, *45*, 657. (d) Feyel, S.; Döbler, J.; Schröder, D.; Sauer, J.; Schwarz, H. *Angew. Chem., Int. Ed.* **2006**, *45*, 4681. (e) Feyel, S.; Schröder, D.; Rozanska, X.; Sauer, J.; Schwarz, H. *Angew. Chem., Int. Ed.* **2006**, *45*, 4677. (f) Das, U.; Raghavachari, K.; Jarrold, C. C. *J. Chem. Phys.* **2005**, *122*, 014313. (g) Wyrwas, R. B.; Yoder, B. L.; Maze, J. T.; Jarrold, C. C. *J. Phys. Chem. A* **2006**, *110*, 2157. (h) Guevara-Garcia, A.; Martinez, A.; Ortiz, J. V. *J. Chem. Phys.* **2007**, *126*, 024309. (i) Zhai, H. J.; Wang, L. S. *J. Am. Chem. Soc.* **2007**, *129*, 3022. (j) Sauer, J. In *Computational Modeling for Homogeneous Catalysis and Biocatalysis*; Morokuma, K., Musaev, J., Eds.; Wiley-VCH: Weinheim, Germany, 2007, in press.
(17) Böhme, D. K.; Schwarz, H. *Angew. Chem., Int. Ed.* **2005**, *44*, 2336.

 10.1021/ja0750874 CCC: $37.00

Sauer and co-worker discovered a series of $(V_2O_5)_n$ polyhedral cage clusters using density functional theory (DFT) calculations previously.[6] A subsequent study on $(V_2O_5)_n^-$ ($n = 2-4$) combining infrared multiple photon dissociation (IRMPD) spectroscopy and DFT calculations confirmed the cage structures and predicted a size-dependent delocalization versus localization of the extra electron in these cluster anions.[13] Another recent IRMPD and DFT study further showed that substitution of V by Ti in bimetallic oxide clusters, $(V_2O_5)_{n-1}(VTiO_5)^-$ ($n = 2-4$) maintains the cage frameworks.[14] The structural robustness of the $(V_2O_5)_n$ cage clusters makes them ideal molecular models for catalytic reactions.[16d] However, the electronic properties of these cage clusters, which are essential to allow a full understanding of their chemical reactivities, have not been examined experimentally.

In the current contribution, we use photoelectron spectroscopy (PES) of size-selected anions, in conjunction with DFT calculations, to probe the electronic structure of the vanadium oxide cage clusters, as well as two 4d and 5d analogues. PES of size-selected anions is a powerful experimental technique to probe the electronic structure of atomic clusters and can yield direct spectroscopic information about the energy gaps and electronic transitions of neutral clusters. However, PES of $(V_2O_5)_n^-$ clusters has been rather challenging because of their relatively high electron binding energies and large energy gaps. For example, the commonly available harmonics of the YAG laser are not sufficient to detach electrons from any $(V_2O_5)_n^-$ clusters. Even the 193 nm (6.424 eV) photons can access only the electronic ground state of these species, while the 157 nm (7.866 eV) photons (the highest photon energy from currently available commercial lasers) are needed to fully reveal their energy gaps.

For the present work, we have measured PES spectra at both 193 and 157 nm for $(V_2O_5)_n^-$ ($n = 2-4$), as well as for two 4d and 5d clusters, $M_4O_{10}^-$ (M = Nb, Ta). Well-resolved spectra have been obtained and are compared with DFT calculations to further confirm the cage structures for both the anions and neutrals of these early transition-metal oxide clusters. The size evolution of the energy gap in the $(V_2O_5)_n^-$ ($n = 2-4$) clusters and the periodic trend in the $M_4O_{10}^-$ (M = V, Nb, Ta) series are presented. The PES data also yield experimental evidence for the predicted d-electron delocalization versus localization in the $(V_2O_5)_n^-$ clusters. Interestingly, the HOMO−LUMO excitation energies in these stoichiometric clusters are observed to be larger than the band gaps of their corresponding bulk oxides. This is most likely due to the unique cage structures of the small clusters and may be relevant to understanding the electronic and structural properties of the oxide surfaces and supported catalysts. It has indeed been shown that the activity of supported vanadium oxide catalysts correlates with the UV−vis absorption edge,[18] and the edge energies reported for vanadium oxide and niobium oxide particles supported on alumina fall in the same range as the HOMO−LUMO excitation energies derived from the current PES results of the gas-phase clusters.

2. Experimental and Computational Methods

2.1. Photoelectron Spectroscopy. The experiments were carried out using a magnetic-bottle PES apparatus equipped with a laser vaporization cluster source, details of which have been described previously.[19,20] Briefly, the transition-metal oxide clusters were produced by laser vaporization of a pure V, Nb, or Ta disk target in the presence of a He carrier gas seeded with 0.5% O_2 and analyzed using a time-of-flight mass spectrometer. The $(V_2O_5)_n^-$ ($n = 2-4$) and $M_4O_{10}^-$ (M = Nb, Ta) clusters of current interest were each mass-selected and decelerated before being photodetached. Two detachment photon energies were used in the current study: 193 nm (6.424 eV) from an ArF excimer laser and 157 nm (7.866 eV) from a F2 excimer laser. Because of the high heat of formation, nascent clusters can contain large amounts of thermal energies. We found previously that under our experimental conditions clusters coming out of the nozzle late are adequately thermalized and are relatively cold, yielding well-resolved PES spectra.[21] Thus, we tried to select such clusters by carefully tuning the timing of the cluster extractions, which has proven to be essential for obtaining high quality PES data. Photoelectrons were collected at nearly 100% efficiency by the magnetic bottle and analyzed in a 3.5 m long electron flight tube. PES spectra were calibrated using the known spectrum of Au^-, and the energy resolution of the PES apparatus was $\Delta Ek/Ek \approx$ 2.5%, that is, ~25 meV for 1 eV electrons.

2.2. Computational Methods. The DFT calculations used the B3LYP functional[22] with triple-ζ valence plus polarization basis sets (TZVP)[23] and the corresponding effective core potentials for Nb and Ta as implemented in TURBOMOLE,[24] the DFT code employed throughout this study. Unrestricted Kohn−Sham calculations were made for the open shell anions. "Vertical" excitation energies of the neutral systems were calculated by performing TDDFT calculations[25] with the ESCF module at the equilibrium structures of the anions. Adiabatic excitation energies were also obtained from SCF calculations for the neutrals in their lowest triplet states. Structures were optimized until Cartesian gradients were smaller than 1×10^{-4} Hartree/Bohr and the energy change was smaller than 1×10^{-6} Hartree. The SCF convergence criterion was 1×10^{-8} Hartree for the energy and 1×10^{-8} au for the root-mean-square of the density (gridsize, m5).

3. Experimental Results

Figure 1 shows the PES spectra of $(V_2O_5)_n^-$ ($n = 2-4$) at 193 and 157 nm. The spectra of $Nb_4O_{10}^-$ and $Ta_4O_{10}^-$ are presented in Figure 2, along with those of $V_4O_{10}^-$ for comparison. For clarity, the 193 nm spectra, which can only reveal the ground-state transitions (X), are shown as insets in both Figures 1 and 2. The 193 nm data are better resolved and yield more accurate electron binding energies. The 157 nm spectra show the ground-state transition as a relatively weak feature, followed by a large energy gap and more intense features at very high binding energies (>6.7 eV). The ground-state vertical detachment energy (VDE) is obtained from the maximum of band X. The VDE of band A can be evaluated for all the species except for $V_8O_{20}^-$, for which only the threshold part of band A is

(18) (a) Khodakov, A.; Olthof, B.; Bell, A. T.; Iglesia, E. *J. Catal.* **1999**, *181*, 205. (b) Chen, K. D.; Bell, A. T.; Iglesia, E. *J. Catal*. **2002**, *209*, 35. (c) Gao, X.; Wachs, I. E. *J. Phys. Chem. B* **2000**, *104*, 1261. (d) Gao, X.; Wachs, I. E.; Wong, M. S.; Ying, J. Y. *J. Catal.* **2001**, *203*, 18.

(19) Wang, L. S.; Cheng, H. S.; Fan, J. *J. Chem. Phys*. **1995**, *102*, 9480.

(20) Wang, L. S.; Wu, H. In *Cluster Materials*; Duncan, M. A., Ed.; Advances in Metal and Semiconductor Clusters, Vol. 4; JAI Press: Greenwich, CT, 1998; pp 299−343.

(21) (a) Wang, L. S.; Li, X. In *Clusters and Nanostructure Interfaces*; Jena, P., Khanna, S. N., Rao, B. K., Eds.; World Scientific: New Jersey, 2000; pp 293−300. (b) Akola, J.; Manninen, M.; Hakkinen, H.; Landman, U.; Li, X.; Wang, L. S. *Phys. Rev. B* **1999**, *60*, R11297. (c) Wang, L. S.; Li, X.; Zhang, H. F. *Chem. Phys*. **2000**, *262*, 53. (d) Zhai, H. J.; Wang, L. S.; Alexandrova, A. N.; Boldyrev, A. I. *J. Chem. Phys*. **2002**, *117*, 7917.

(22) (a) Becke, A. D. *J. Chem. Phys*. **1993**, *98*, 5648. (b) Lee, C.; Yang, W.; Parr, R. G. *Phys. Rev. B* **1988**, *37*, 785.

(23) Schäfer, A.; Huber, C.; Ahlrichs, R. *J. Chem. Phys*. **1994**, *100*, 5829.

(24) (a) Ahlrichs, R.; Bär, M.; Häser, M.; Horn, H.; Kölmel, C. *Chem. Phys. Lett*. **1989**, *162*, 165. (b) Treutler, O.; Ahlrichs, R. *J. Chem. Phys*. **1995**, *102*, 346. (c) Eichkorn, K.; Treutler, O.; Öhm, H.; Häser, M.; Ahlrichs, R. *Chem. Phys. Lett*. **1995**, *242*, 652.

(25) (a) Bauernschmitt, R.; Häser, M.; Treutler, O.; Ahlrichs, R. *Chem. Phys. Lett.* **1997**, *264*, 573. (b) Furche, F.; Ahlrichs, R. *J. Chem. Phys.* **2002**, *114*, 7433.

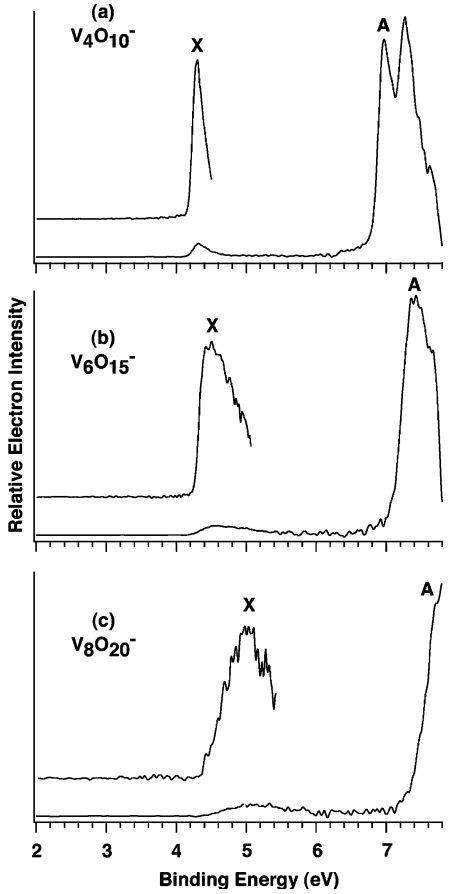

Figure 1. Photoelectron spectra of (a) $V_4O_{10}^-$, (b) $V_6O_{15}^-$, and (c) $V_8O_{20}^-$ taken at 193 nm (6.424 eV) and 157 nm (7.866 eV) photon energies. The 193 nm spectra are shown as insets.

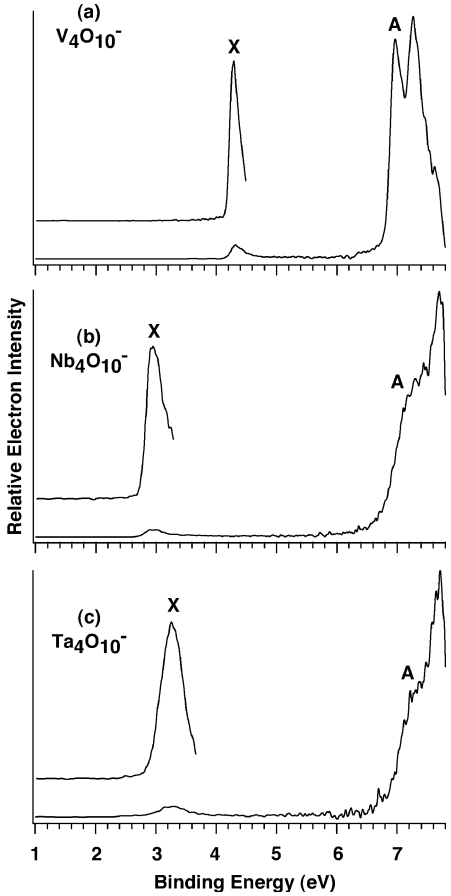

Figure 2. Photoelectron spectra of $Nb_4O_{10}^-$ (b) and $Ta_4O_{10}^-$ (c) at 193 and 157 nm, compared to whose of $V_4O_{10}^-$. The 193 nm spectra are shown as insets.

observed (Figure 1c). Since no vibrational structures are resolved, the ground-state adiabatic detachment energy (ADE), that is, the electron affinity of the neutral species, is evaluated by drawing a straight line along the leading edge of band X and then adding the instrumental resolution to the intersection with the binding energy axis. Although this is an approximate procedure, we are able to obtain a set of consistent ADEs from the well-defined spectral onsets of band X at different photon energies. The ADE for band A is evaluated from the 157 nm spectra following the same procedure. The obtained ADEs and VDEs are given in Table 1.

The ground-state ADEs for all three $(V_2O_5)_n^-$ clusters are quite high with a relatively small size-dependence, increasing only by 0.06 eV for $n = 3$ and 0.13 eV for $n = 4$. The ADE of band A is more sensitive to cluster size and increases by ~0.25 eV per V_2O_5 unit from $n = 2$ to 4. For the $M_4O_{10}^-$ series (Figure 2), $Nb_4O_{10}^-$ and $Ta_4O_{10}^-$ show nearly identical PES spectra with relatively low electron binding energies for the ground-state transition in comparison to $V_4O_{10}^-$. The electron binding energies of band A are similar for all three $M_4O_{10}^-$ clusters.

The difference between the ADE and VDE of the ground-state transition defines a reorganization energy (E_{reorg}, Table 1), which characterizes the anion-to-neutral structural change upon photodetachment. The X band for the three $M_4O_{10}^-$ clusters is relatively sharp and broadens slightly going down the periodic table, suggesting only minor structural changes between the ground states of $M_4O_{10}^-$ and their corresponding neutrals. The X bandwidth increases significantly as a function of size for the $(V_2O_5)_n^-$ clusters, resulting in a reorganization energy of 0.20 eV for $n = 3$ and 0.61 eV for $n = 4$ and suggesting more significant anion-to-neutral structural relaxation for the larger clusters.

The overall PES patterns of all the five species are characteristic of stable closed-shell neutrals with large energy gaps between their highest occupied molecular orbitals (HOMOs) and lowest unoccupied molecular orbitals (LUMOs). The extra electron in the anions occupies the LUMO of the neutral clusters, yielding a singly occupied MO (SOMO) for the anions and giving rise to the X band in the PES spectra. The A band involves electron detachment from those orbitals, which corresponds to the neutral HOMO. Thus, the ADE difference between bands X and A, as also given in Table 1, provides an experimental measure of the HOMO−LUMO gap for the neutral clusters, although strictly speaking it represents the singlet−triplet excitation energies in the neutral systems. The HOMO−LUMO gap shows a moderate size-dependence from 2.58 → 2.78 → 2.90 eV along the $(V_2O_5)_n$ ($n = 2-4$) series. For the $M_4O_{10}^-$ clusters, the 4d and 5d species possess nearly identical HOMO−LUMO gaps, which are much larger than the 3d species.

4. Computational Results

The structures of the $(V_2O_5)_n^-$ ($n = 2-4$) anions have been optimized previously.[13] The respective neutral systems are optimized in the current work, resulting in highly symmetric structures with T_d, D_{3h}, and D_{4h} symmetries, respectively, as

Table 1. Observed Vertical (VDE) and Adiabatic (ADE) Detachment Energies for Detachment Transitions to the Ground State (X) and the First Excited State (A), Reorganization Energies (E_{reorg}), and the X−A Energy Gaps for $(V_2O_5)_n^-$ ($n = 2-4$), $Nb_4O_{10}^-$, and $Ta_4O_{10}^-$.[a]

	band X			band A			
	ADE[b,c]	VDE[b]	E_{reorg}	ADE[b]	VDE[b]	X–A gap[b]	bulk band gap
$V_4O_{10}^-$	4.26(3)	4.31(3)	0.05	6.84(3)	6.97(3)	2.58(3)	
$V_6O_{15}^-$	4.32(3)	4.52(10)	0.20	7.10(3)	7.41(3)	2.78(3)	2.3[d]; 2.1−2.9[e]
$V_8O_{20}^-$	4.45(5)	5.06(10)	0.61	7.35(5)		2.90(5)	
$Nb_4O_{10}^-$	2.87(3)	2.96(3)	0.09	6.75(10)	∼7.2	3.88(10)	3.4[f]; 3.8[g]
$Ta_4O_{10}^-$	2.98(4)	3.24(3)	0.26	6.85(10)	∼7.2	3.87(10)	3.5−4.5[h]

[a] The bulk band gaps of the M_2O_5 (M = V, Nb, Ta) oxides are included for comparison. All energies are in eV. [b] Numbers in parentheses represent the experimental uncertainties in the last digits. [c] Electron affinity of the neutral species. [d] From ref 31. [e] VO_x supported on Al_2O_3 (ref 18). [f] From ref 33. [g] NbO_x supported on Al_2O_3 (ref 18). [h] From ref 34.

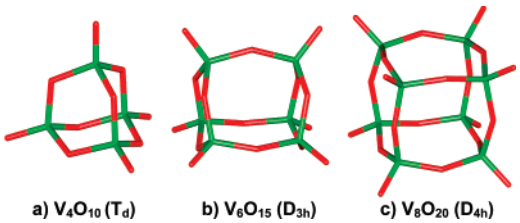

Figure 3. The optimized structures of (a) V_4O_{10}, (b) V_6O_{15}, and (c) V_8O_{20}.

Table 2. B3LYP Results for Vertical (VDE) and Adiabatic (ADE) Detachment Energies to the Ground (X) and First Excited State (A), the Reorganization Energies (E_{reorg}) for the X Band, and the X−A Gap[a]

		X			A		
		ADE	VDE	E_{reorg}	ADE	VDE[b]	X–A gap[c]
$V_4O_{10}^-$	D_{2d} $^2B_1$	4.41	4. 49	0.08	6.56	7.13	2.15
$V_6O_{15}^-$	C_s $^2A'$	4.55	5.28	0.73	6.80	7.63	2.25
	C_{2v} $^2A_2$	4.45	4.75	0.30			
$V_8O_{20}^-$	C_s $^2A''$	4.68	5.48	0.80	7.02	7.86	2.34
	C_{2v} $^2A_2$	4.59	5.00	0.41			
$Nb_4O_{10}^-$	D_{2d} $^2B_1$	3.24	3.34	0.10	6.76	6.87	3.52
$Ta_4O_{10}^-$	D_2 ^2A	2. 78	2. 87	0.09	6.65	6.80	3.87

[a] All energies are in eV. The symmetries for the neutral clusters: T_d for M_4O_{10} (M = V, Nb, Ta); D_{3h} for V_6O_{15}; D_{4h} for V_8O_{20}. [b] VDE(A) = VDE(X) + excitation energy calculated with TDDFT at the structure of the cluster anion. [c] ΔE_{SCF}, excited (triplet) state optimized (SCF).

shown in Figure 3. Other noncage clusters have been considered previously,[6a] but they are much higher in energy.

The lowest energy structures of Nb_4O_{10} and Ta_4O_{10} are also of T_d symmetry similar to V_4O_{10} (Figure 3a) and their corresponding anions are of D_{2d} and D_2 symmetry, respectively. In $Ta_4O_{10}^-$, the distortion from D_{2d} to D_2 is associated with a very small energy change of 1.5 meV (0.035 kcal/mol) only. Application of the genetic algorithm as described by Sierka et al.[26] and applied to $V_nO_m^-$ anions[27] did not yield any other structures of lower symmetries or energies.

Table 2 shows the calculated ADE and VDE values with respect to the ground state (X) and the first excited state (A) of the respective neutrals. In the anions, the extra electron occupies the neutral LUMO, which consists primarily of the metal d orbitals (Figures 4−6). As schematically shown in Figure 7, detachment from this SOMO results in the lowest binding energy feature X in the PES spectra, whereas detachment of an electron from the filled HOMO (mainly of O2p states, Figures 4−6) leads to an excited state of the neutral (feature A, corresponding

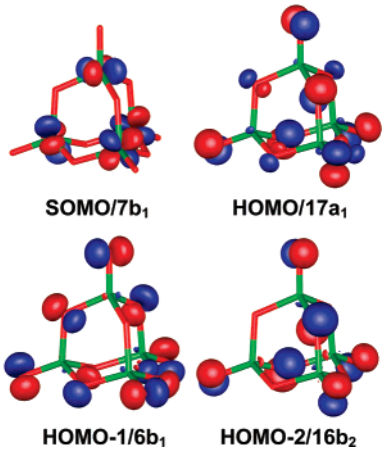

Figure 4. The 3d-based SOMO and the top O2p-derived HOMOs of $V_4O_{10}^-$.

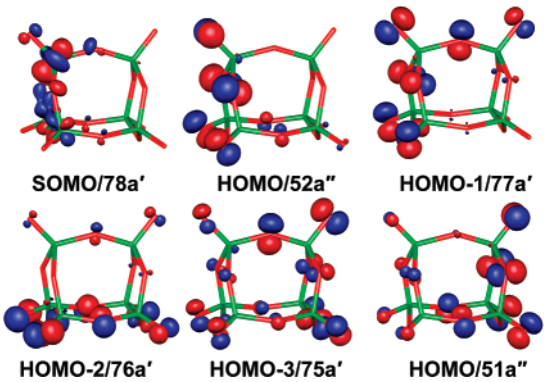

Figure 5. The 3d-based SOMO and the top O2p-derived HOMOs of $V_6O_{15}^-$.

to ligand-to-metal charge transfer). The VDE of band X is obtained as the difference between the DFT energies of the neutral and the anion at the equilibrium structure of the anion. The VDE of band A is obtained from the VDE of band X by adding the energy for the excitation of the neutral in its lowest triplet state at the equilibrium structure of the anion. As there are many O2p-based states within a narrow energy interval (a few O2p-type orbitals near the HOMO are shown in Figures 4−6), it does not come as a surprise that there is a multitude of energetically close excited states, all of ligand-to-metal charge-transfer character. Table 3 shows the lowest excited states, both singlet and triplet, that correspond to electron detachment from doubly occupied O2p-type orbitals of the anions (Figures 4−6) as obtained from TDDFT.

Optimization of the neutral oxide clusters yields the total energies needed for calculating the ADE values of the X band,

(26) Sierka, M.; Döbler, J.; Sauer, J.; Santambrogio, G.; Brümmer, M.; Wöste, L.; Janssens, E.; Meijer, G.; Asmis, K. R. *Angew. Chem., Int. Ed.* **2007**, *46*, 3372.
(27) Santambrogio, G.; Brümmer, M.; Wöste, L.; Döbler, J.; Sauer, J.; Meijer, G.; Asmis, K., to be submitted for publication.

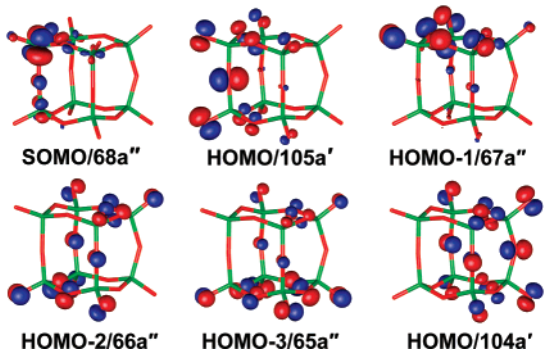

Figure 6. The 3d-based SOMO and the top O2p-derived HOMOs of $V_8O_{20}^-$.

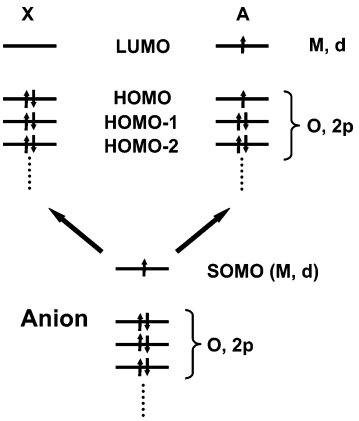

Figure 7. Schematic diagram showing two detachment channels from the SOMO and HOMO of the cluster anions.

Table 3. Excitation Energies (eV) for the Neutrals at the Structure of the Respective Anions as Obtained by TDDFT. "Adiabatic" Excitation Energies Obtained from SCF Calculations for the Anion and the Neutral Are Also Given

	state	TDDFT	transition	ionization from	optimized	SCF
			V_4O_{10} (D_{2d})[a]			
1	$^3A_1$	2.64	$6b_1-7b_1$	HOMO-1	C_1-^{3}A	2.15
2	$^3B_1$	2.70	$17a_1-7b_1$	HOMO	C_s-^{3}A″	2.16
4	$^1B_1$	2.75	$17a_1-7b_1$	HOMO		
6	$^1A_1$	2.81	$6b_1-7b_1$	HOMO-1		
9	$^3A_2$	2.90	$16b_2-7b_1$	HOMO-2		
			V_6O_{15} (C_s)[a]			
1	^{3}A′	2.35	77a′−78a′	HOMO	C_s-^{3}A′	2.25
2	^{3}A″	2.36	52a″−78a′	HOMO-1	C_s-^{3}A″	2.51
3	^{3}A′	2.39	75a′−78a′	HOMO-3		
4	^{1}A′	2.40	77a′−78a′	HOMO		
5	^{1}A″	2.42	52a″−78a′	HOMO-1		
6	^{1}A′	2.48	75a′−78a′	HOMO-3		
			V_8O_{20} (C_s)[a]			
1	^{3}A′	2.39	67a″−68a″	HOMO-1	C_s-^{3}A′	2.33
2	^{3}A″	2.39	105a′−68a″	HOMO		
3	^{3}A′	2.39	66a″−68a″	HOMO-2		
4	^{3}A′	2.40	65a″−68a″	HOMO-3		
5	^{3}A″	2.41	104a′−68a″	HOMO-4		
6	^{1}A′	2.41	67a″−68a″	HOMO-1		
7	^{1}A″	2.41	105a′−68a″	HOMO		
8	^{1}A′	2.43	66a″−68a″	HOMO-2		
9	^{1}A″	2.47	104a′−68a″	HOMO-4		
10	^{1}A′	2.50	65a″−68a″	HOMO-3		

[a] Calculated at the structure of the cluster anion.

as given in Table 2. All neutrals have the full symmetry expected for polyhedral structures of identical building units (Figure 3, see also ref 6) for V_6O_{15} and V_8O_{20}. Since the $V_6O_{15}^-$ and $V_8O_{20}^-$ anions have broken symmetry (C_s) equilibrium structures, they exhibit much larger reorganization energies upon electron detachment (0.73 and 0.80 eV, respectively) than any of the $M_4O_{10}^-$ clusters (0.08−0.10 eV). For $V_6O_{15}^-$ and $V_8O_{20}^-$ there also exist C_{2v} structures that represent transition structures (saddle points on the potential-energy surface) for the interconversion of two equivalent C_s structures.[27] Since the barrier is very low, the C_{2v} structure might be a better representation of the average structure of the anion even in the vibrational ground state. Therefore, results for these C_{2v} anion structures are also included in Table 2. The reorganization energies for the C_{2v} structures are smaller, 0.30 and 0.41 eV, because they represent smaller geometry changes relative to the neutral clusters, but they are still significantly larger than that for $V_4O_{10}^-$.

The ADEs for the A band are obtained by taking the difference between the energy of the optimized structure of the neutral in its first excited (triplet) state and the ground-state energy of the anion. This is the equivalent of adding the first adiabatic excitation energy of the neutral to the first ADE (X band). The first excited triplet states all have reduced symmetries, C_1 for V_4O_{10} and C_s for V_6O_{15} and V_8O_{20}.

5. Discussion

5.1. $(V_2O_5)_n^-$ (n = 2−4): Evolution of the Electronic Structure as a Function of Size. The electron binding energies of the $(V_2O_5)_n^-$ (n = 2−4) clusters are all quite high (>4.2 eV), indicating that the neutral $(V_2O_5)_n$ cages are highly electronegative despite the fact that these are closed-shell and stoichiometric species. The ADE of the X band seems to show very weak size-dependence, consistent with the nature of the SOMO (Figures 4−6), which is composed mainly of vanadium 3d states. The ADE of the A band exhibits a stronger size-dependence, increasing by ~0.25 eV per V_2O_5 unit. This observation suggests that the O2p-derived orbitals in $(V_2O_5)_n$ are more sensitive to the degree of aggregation, probably due to increased electrostatic interactions in the larger clusters. The stabilization of the O2p-derived states as a function of size, which has also been observed in the $(TiO_2)_n^-$ clusters recently,[16i] is the main cause for the increase of the HOMO−LUMO gap in $(V_2O_5)_n$ as a function of size. For the $(TiO_2)_n$ clusters, it was observed that the HOMO−LUMO gap already reaches the bulk band gap for n > 6.[16i]

The evolution of the HOMO−LUMO gap suggests that the $(V_2O_5)_n$ clusters should exhibit size-dependent chemical reactivities. The smaller gap in V_4O_{10} suggests that it should be more reactive, in particular for those reactions involving ligand-to-metal charge transfers, such as H-abstraction reactions, $V^V = O + HR \rightarrow V^{IV}-OH + \bullet R$.[16j] The $V_4O_{10}^+$ cation has been shown recently to be able to abstract a H from CH_4 via a barrierless reaction.[16d]

5.2. $M_4O_{10}^-$ (M = V, Nb, Ta): Periodic Trend. As shown in Figure 2, the $Nb_4O_{10}^-$ and $Ta_4O_{10}^-$ species exhibit almost identical PES spectra, which display some significant differences from those of $V_4O_{10}^-$. The spectra of $V_4O_{10}^-$ are sharper with higher electron binding energies and a smaller energy gap. Thus, despite the similarity in their symmetry and electronic structure, the spectrum of the 3d system seems to be quite different from those of its 4d/5d counterparts. Similar trend from 3d to 4d/5d transition-metal oxides has also been observed in our previous PES work for group VI elements, MO_n^- and $M_2O_7^{2-/-}$ (M =

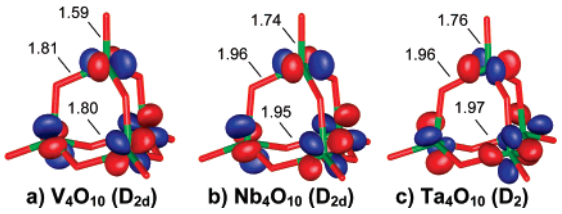

Figure 8. Comparison of the SOMO and structures of $V_4O_{10}^-$, $Nb_4O_{10}^-$, and $Ta_4O_{10}^-$. All bond lengths are in Å.

Cr, Mo, W),[16b,28,29] where the Cr−O systems are found to be different from the corresponding Mo/W oxide systems. In general the 3d orbitals are more contracted than the 4d/5d orbitals, which result in the higher electron binding energies in the $V_4O_{10}^-$ cluster because the extra electron resides in an almost pure 3d-type MO.

In Figure 8 we compare the SOMO and key structural parameters for the three $M_4O_{10}^-$ clusters. Indeed, we see that both the bridging V−O and terminal V═O bond distances are much shorter than the corresponding Nb−O/Nb═O and Ta−O/Ta═O bond distances, consistent with the relative atomic sizes. The smaller $V_4O_{10}^-$ cage suggests that there may be more significant d−d interactions, providing further stabilization to the extra electron. This stabilization of the LUMO in V_4O_{10} also leads to a reduced HOMO−LUMO gap, in comparison to that in Nb_4O_{10} and Ta_4O_{10}. Again, this difference in the HOMO−LUMO gap implies that V_4O_{10} should be more reactive than its Nb/Ta counterparts.

The spectra of $Nb_4O_{10}^-$ and $Ta_4O_{10}^-$ are both broader than those of $V_4O_{10}^-$ (Figure 2), indicating more significant geometry changes between the anion and neutral final states for the Nb and Ta clusters. This observation is consistent with our theoretical calculations. The neutrals of all three M_4O_{10} clusters possess T_d symmetry (Figure 3a). In the anion, the symmetry is lowered to D_{2d} for $V_4O_{10}^-$ and $Nb_4O_{10}^-$ and D_2 for $Ta_4O_{10}^-$. However, the structural changes are relatively minor for $V_4O_{10}^-$ in comparison with $Nb_4O_{10}^-$ and $Ta_4O_{10}^-$. Hence, both our experimental and theoretical results indicate that the smaller V_4O_{10} cage is more rigid.

5.3. Comparison of Experimental and Theoretical Electron Detachment Energies. The calculated detachment energies for all five clusters are given in Table 2. For $V_4O_{10}^-$, the calculated ADE (4.41 eV) and VDE (4.49 eV) for the ground-state transition are in very good agreement with the experimental values (4.26 and 4.31 eV, respectively). The theoretical calculations overestimate the ADE and VDE by about 0.15−0.18 eV, not unexpected for the level of theory used. For the two larger clusters $V_6O_{15}^-$ and $V_8O_{20}^-$, much larger discrepancies are observed. The calculated ADEs for the ground-state C_s structures are higher than the experimental values by ~0.23 eV. However, the calculated VDEs seem to be much higher than the experimental data, by 0.76 and 0.42 eV for $V_6O_{15}^-$ and $V_8O_{20}^-$, respectively. We further computed the ADE and VDE values for the C_{2v} structures of both clusters, which are low-energy saddle points connecting two equivalent C_s structures. As can be seen in Table 2, the calculated ADEs (4.45 eV for $V_6O_{15}^-$ and 4.59 eV for $V_8O_{20}^-$) for the C_{2v} structures are in good agreement with the experimental values (4.32 and 4.45 eV). More importantly, the calculated VDEs for the C_{2v} structures (4.75 and 5.00 eV for $V_6O_{15}^-$ and $V_8O_{20}^-$, respectively) agree well with the experimental data (4.52 and 5.06 eV, respectively). These results suggest that under our experimental conditions (close to room temperature) the structures for $V_6O_{15}^-$ and $V_8O_{20}^-$ are likely to be C_{2v} on average.

The larger reorganization energies for the ground-state transitions, both observed (Table 1) and calculated (Table 2), for $V_6O_{15}^-$ and $V_8O_{20}^-$ compared to $V_4O_{10}^-$ provide further evidence for a size-dependent symmetry breaking because of d-electron localization in the SOMO of the larger clusters (Figures 4−6).[13]

We also calculated the ADEs and VDEs to the first excited states of the neutral clusters (Table 2), corresponding to the A band in the PES spectra. In the cases of $V_6O_{15}^-$ and $V_8O_{20}^-$, calculations were done only for the global minimum C_s structures. We found that the calculations underestimated the ADE values for the A band by about 0.28−0.33 eV, whereas the calculated VDE values for the A band seem to agree better with the experiment. The underestimation of the ADEs for the A band also led to lower calculated HOMO−LUMO gaps, as shown in Table 2, although the size dependence is consistent with the experimental observation.

For the ground-state transitions of $Nb_4O_{10}^-$ and $Ta_4O_{10}^-$, we found much larger discrepancies between the calculated electron binding energies (Table 2) and the experimental measurements. This is perhaps not too surprising because of the increasing importance of the relativistic effects for the 4d and 5d systems, which are only partially accounted for in the pseudopotentials in the current theoretical methods.

The PES features in the high binding energy range are all due to detachment from fully occupied O2p-type MOs. There is a high density of such MOs, which also increases rapidly with cluster size. Experimentally, we were able to resolve two peaks in this spectral range for $V_4O_{10}^-$ and only a broad band for $V_6O_{15}^-$, as shown in Figure 1. We computed, for the three neutral $(V_2O_5)_n$ ($n = 2-4$) clusters, the energies of the first few transitions corresponding to excitations of the occupied O2p electrons, as shown in Table 3. Indeed, a very high density of states are obtained, in particular, for the $n = 3$ and 4 cases. Even for V_4O_{10}, many states are obtained within an energy range of ~0.3 eV, suggesting the two peaks in the 157 nm spectrum of $V_4O_{10}^-$ (Figure 1a) may also contain several overlapping detachment transitions.

5.4. Comparison with Bulk Oxides. The metal−oxygen bond in the group VB metal oxides is quite ionic and one can view the metal atom to donate all its valence electrons to the O2p orbitals. In the stoichiometric oxides, the O2p orbitals form the fully occupied valence band and the empty metal sd orbitals form the conduction band with a large band gap. Bulk V_2O_5 is well characterized to adopt a layered structure with a band gap of 2.3 eV.[2,30,31] The layers are made up of double ribbons, in which the V atoms are pentacoordinated within a layer in a tetragonal pyramidal arrangement with an additional weak

(28) Gutsev, G. L.; Jena, P.; Zhai, H. J.; Wang, L. S. *J. Chem. Phys.* **2001**, *115*, 7935.
(29) Zhai, H. J.; Huang, X.; Waters, T.; Wang, X. B.; O'Hair, R. A. J.; Wedd, A. G.; Wang, L. S. *J. Phys. Chem. A* **2005**, *109*, 10512.
(30) Krishna, M. G.; Bhattacharya, A. K. *Mater. Sci. Eng. B* **2001**, *86*, 41.
(31) (a) Van Hieu, N.; Lichtman, D. *J. Vac. Sci. Technol.* **1981**, *18*, 49. (b) Cogan, S. F.; Nguyen, N. M.; Perrotti, S. J.; Rauh, R. D. *J. Appl. Phys.* **1989**, *66*, 1333. (c) Moshfegh, A. Z.; Ignatiev, A. *Thin Solid Films* **1991**, *198*, 251. (d) Ramana, C. V.; Smith, R. J.; Hussain, O. M.; Chusuei, C. C.; Julien, C. M. *Chem. Mater.* **2005**, *17*, 1213.

interlayer bond, resulting in a distorted 6-fold coordination.[32] Bulk Nb_2O_5 and Ta_2O_5 oxides form a number of polymorphs and are less well-characterized in comparison to V_2O_5. The band gap of Nb_2O_5 is known to be 3.4 eV.[2,30,33] However, the band gap of Ta_2O_5 in the literature spreads over a wide energy range from 3.5 to 4.5 eV.[2,34]

It would be interesting to compare the observed HOMO−LUMO gaps to the bulk band gaps, even though the atoms in the clusters are all on the surface. As shown in Table 1, the observed energy gaps for the $(V_2O_5)_n^-$ clusters exceed that of the bulk. Similarly, the observed energy gap for $Nb_4O_{10}^-$, to some extent for $Ta_4O_{10}^-$ as well, is also greater than that of the bulk oxide. In a recent PES study on $(TiO_2)_n^-$ ($n = 1-10$) clusters, we observed that the HOMO−LUMO gaps in the TiO_2 clusters increase as a function of size and reach that of the bulk value for $n = 6$.[16i] However, the HOMO−LUMO gap in the small TiO_2 clusters never exceeds the bulk value. The current observation of the large HOMO−LUMO gaps in the group VB metal oxide clusters relative to their bulk oxides is surprising. This is very likely due to their unique polyhedral cage structures, in which the metal centers are tetracoordinated with one terminal O atom and three bridging O atoms. This coordination environment differs substantially from the bulk oxides, inducing the observed size effect in the HOMO−LUMO gaps.

The enlarged energy gaps in the cage clusters may also have implications for oxide surfaces and catalysts. It has been reported from surface studies that supported group VB metal oxides usually possess significantly greater band gaps than the bulk.[2,18] However, the exact identity of the surface species or the origin of the observation is not well understood. The current observation of the enlarged energy gaps in the gas-phase clusters may be related to the observation on the bulk surfaces, implying that the highly stable cage species may be present on oxide surfaces and play a role in catalysis. The current observation also seems to contradict a notion in surface chemistry, which says the band gap of surface species of the group VB oxides decreases with its number of nearest oxide neighbors and that the isolated monomers possess the highest energy gap.[2] It appears that this notion needs to be revised in light of the current observation.

6. Conclusions

In conclusion, we have studied the electronic properties of two series of group VB oxide clusters, $(V_2O_5)_n^-$ ($n = 2-4$) and $M_4O_{10}^-$ (M = V, Nb, Ta), via photoelectron spectroscopy and density functional calculations. Well-resolved photoelectron spectra were obtained and compared with computational data, further confirming the polyhedral cage structures for these oxide clusters in both the anionic and neutral charge states. Large HOMO−LUMO gaps were observed for all clusters and they increase with cluster size for the $(V_2O_5)_n$ series. The HOMO−LUMO gaps in Nb_4O_{10} and Ta_4O_{10} are similar and they are larger than that in V_4O_{10}. The HOMO−LUMO gaps of all these clusters are shown to be larger than the band gaps in the corresponding bulk oxides, which are ascribed to their unique cage structures with different coordination environment than the bulk. The first PES band for the $(V_2O_5)_n^-$ clusters was observed to become broader, consistent with the predicted transition from electron delocalization for $n = 2$ to localization for $n > 2$. Insight into the bulk oxide surfaces and the size-dependent reactivities is also obtained.

Acknowledgment. The experimental work carried out in Washington was supported by the Chemical Sciences, Geosciences and Biosciences Division, Office of Basic Energy Sciences, U.S. Department of Energy (DOE) under Grant No. DE-FG02-03ER15481 (catalysis center program) and was performed at the W. R. Wiley Environmental Molecular Sciences Laboratory, a national scientific user facility sponsored by DOE's Office of Biological and Environmental Research and located at Pacific Northwest National Laboratory, operated for DOE by Battelle. The theoretical work done in Berlin was supported by the Deutsche Forschungsgemeinschaft (SFB 546). L.S.W. gratefully acknowledges the support by the Alexander von Humboldt Foundation, which makes this collaboration possible.

JA0750874

(32) (a) Enjalbert, R.; Galy, J. *Acta Crystallogr., Sect. C: Cryst. Struct. Commun.* **1986**, *42*, 1467. (b) Bystrom, A.; Wilhelmi, K. A.; Brotzen, O. *Acta Chem. Scand.* **1950**, *4*, 1119.

(33) (a) Duffy, M. T.; Wang, C. C.; Waxman, A.; Zaininger, K. H. *J. Electrochem. Soc.* **1969**, *116*, 234. (b) Yoshimura, K.; Miki, T.; Iwama, S.; Tanemura, S. *Thin Solid Films* **1996**, *281*, 235.

(34) (a) Apker, L.; Taft, E. A. *Phys. Rev.* **1952**, *88*, 58. (b) Khawaja, E. E.; Tomlin, S. G. *Thin Solid Films* **1975**, *30*, 361. (c) Tepehan, F. Z.; Ghodsi, F. E.; Ozer, N.; Tepehan, G. G. *Solar Energy Mater. Solar Cells* **1997**, *46*, 311. (d) Ghodsi, F. E.; Tepehan, F. Z. *Sol. Energy Mater. Sol. Cells* **1999**, *59*, 367. (e) Afanas'ev, V. V.; Stesmans, A.; Zhao, C.; Caymax, M.; Rittersma, Z. M.; Maes, J. W. *Appl. Phys. Lett.* **2005**, *86*, 072108.